Electronic Supplementary Material (ESI) for Journal of Materials Chemistry C.

Supplementary Information

Orientation Preference Control: A Novel Approach for Tailoring Molecular Electronic Functionalities

Xintai Wang,[a,b,c,†] Xiaoying Li, [a*] Shanglong Ning,[b,†] and Ali Ismael[d*,e,†]

*To whom correspondence should be addressed. e-mail: k.ismael@lancaster.ac.uk

Table of Contents:

1. Experimental details:

1.1 Molecule Synthesis:

Synthesis of molecules were according to our previous published paper [1].

1.2 Junction Formation:

Junction formation were according to our previous published paper, detailed procedure was as following [2]:

1.2.1 Device Fabrication:

The micro-well samples were fabricated on p-doped silicon wafers with a layer of 300 nm native thermal silicon oxide. A standard cleaning method was applied to clean the surface before any photolithography process. The cleaning procedure starts with 5-minute immersion in acetone followed by a 2-minute immersion in propan-2-ol (IPA) to remove acetone residue.

The first photolithography step deposited gold fingers in the central area. A double-layer resist was used to achieve clean lift-off and precise edges. The bottom layer was formed by spinning LOR 5B (7000 rpm, 60 s) and the top layer was formed by spinning positive Shipley 1805 photoresist (S1805, 5500 rpm, 60 s). Directly after coating with LOR 5B the sample was soft-baked for 10 minutes at 180 ^{o}C to stabilize the film and improve the adhesion. After spinning the S1805, the samples were baked at 110 ^{o}C for 2 minutes. The UV exposure time was 7.5 seconds; afterwards, the sample was developed in MICROPOSIT MF-319 developer for 20 seconds and then rinsed in DI water. Once the finger pattern had been developed, 5 nm titanium and 20 nm gold were evaporated onto the surface. SVC-14 positive photoresist stripper was used to lift off the unwanted metal.

A series of micro-wells was formed on top of the fingers by selectively etching holes in a 25 nm layer of aluminium oxide. First, atomic-layer deposition was used to deposit a high-quality layer of aluminium oxide with a precise thickness. Using photolithography, holes were opened up in the resist and buffered hydrofluoric acid was then used to etch through the aluminium oxide below, stopping at the gold. Once the micro-wells were formed, S1805 was spun on, to protect the common contacts and gate electrode, and it was removed over the micro-well region using photolithography to allow molecule assembly on the unprotected gold.

A flow chart of device fabrication is shown below:

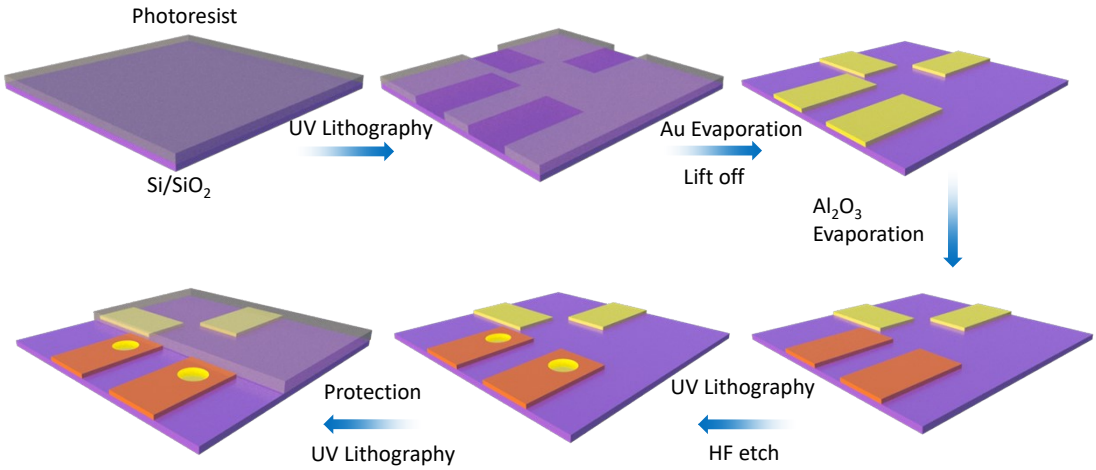

Figure S1. Flow chart of micro-well device fabrication.

1.2.2 Device pre-treatment:

Each device after fabrication was washed with DI water (R>10 MΩ) several times to eliminate any possible metal/salt contaminants, then immersed in hot dimethylformamide (DMF, Sigma-Aldrich, 99.8%, 90 ^{o}C) for 20 minutes to wash off organic contaminants. The device after washing was rinsed in ethanol 3-4 times, and then rinsed in DMF before being put into the chosen solution of molecules to form a SAM.

1.2.3 SAM growth:

1.2.3.1 Growth of SAM 1 and 3

We modified the standard method for SAM growth [3]. The solution of molecules was prepared by dissolving target molecules (molecule 1 and 2) in 10mL DMF (Sigma-Aldrich, 99.8%) with a concentration of 1 mM. The solution was ultra-sonicated for 10 minutes to dissolve the molecules completely. The device after pre-treatment was immersed in this solution for 30 minutes, washed with DMF, ethanol (EtOH), and IPA 3-4 times and re-immersed in the solution. This process was repeated 4 to 5 times, and after that, the device was immersed in the solution for 24-48 hours for SAM growth and self-organisation. Our experiments suggest this type of 'stepwise' self-assembly helps to cure the pinholes in the SAM and decreases the possibility of short circuits. The device after SAM growth was rinsed with DMF, ethanol and IPA 3-4 times to eliminate physiosorbed molecules, and dried at 30^{o}C. Finally, the S1805 layer protecting the contacts was washed off with acetone and then IPA.

1.2.3.2 Growth of SAM 2 and 4

Acetyl deprotection procedure follows the protocol suggested by Millipore Sigma with small modification. The solution of molecules was prepared by dissolving target molecules (molecule 1 and 2) in 10mL DMF (Sigma-Aldrich, 99.8%) with a concentration of 1 mM. 100μL NaOH stock solution (1M) was added to molecular solution dropwise, wait for 2 hours and add 100μL 1M HCL

solution to neutralize the solution. Later SAMs growth procedure were the same as 1.2.3.1, but device will be washed in miliQ water for several times with mild ultrasonication (40W) for 15 minutes after taking out from solution to wash off the ion remain. To ensure the salt in solution will influence the device, the electric measurement on device after SAM growth without graphene transfer was measured by a home-made probe station, and no current leakage was observed.

1.2.4 Graphene transfer:

Single-layered graphene on copper (Graphene supermarket, Graphene on 1 side was used in this work. The copper etching procedure followed the standard recipe for graphene transfer [4]: 0.1 M ammonium persulfate (APS) was dissolved in water as etchant solution. 4% poly(methyl methacrylate) (PMMA) was spin coated on copper with graphene (6000 rpm, 1 min) as a protection layer, and incubated at 150 ^{o}C for 1 minute to allow solvent evaporation. After heating, PMMA/graphene/Cu was transferred into the etchant solution for Cu etching. The etching process takes 18-24 hours. After copper etching, the graphene was transferred into clean DI water for 6 times to wash off remaining APS, and the PMMA-protected graphene was transferred onto our device with SAM by 'fishing'.

The device after graphene transfer was incubated in high vacuum (10^{-7} mbar) for 24 hours to remove residual water. After this drying stage, the PMMA was washed off by immersing the device in acetone, and rinsing under acetone gently with further acetone from a glass pipette. This procedure was repeated several times, and the device after rinsing was immersed in acetone overnight to eliminate PMMA residue. Below is a flow chart for graphene transfer:

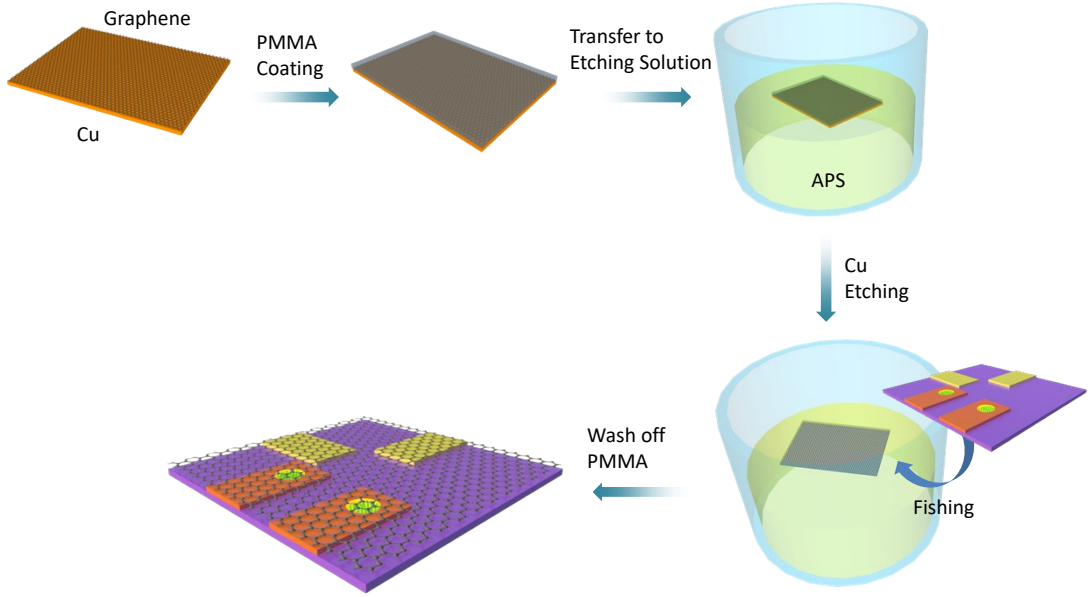

Figure S2. Flow chart of transferring graphene on top of a micro-well device

1.2.5 Graphene patterning:

The device after PMMA removal was coated with photoresist (S1805) by spin coating, and

dried in high vacuum overnight. UV-lithography was used to pattern graphene stripes covering each set of micro-wells, and the un-protected graphene was removed with an RF (Radio Frequency) asher to avoid short-circuits.

The flow chart below (Fig. S3) shows these steps and corresponding AFM characterization images:

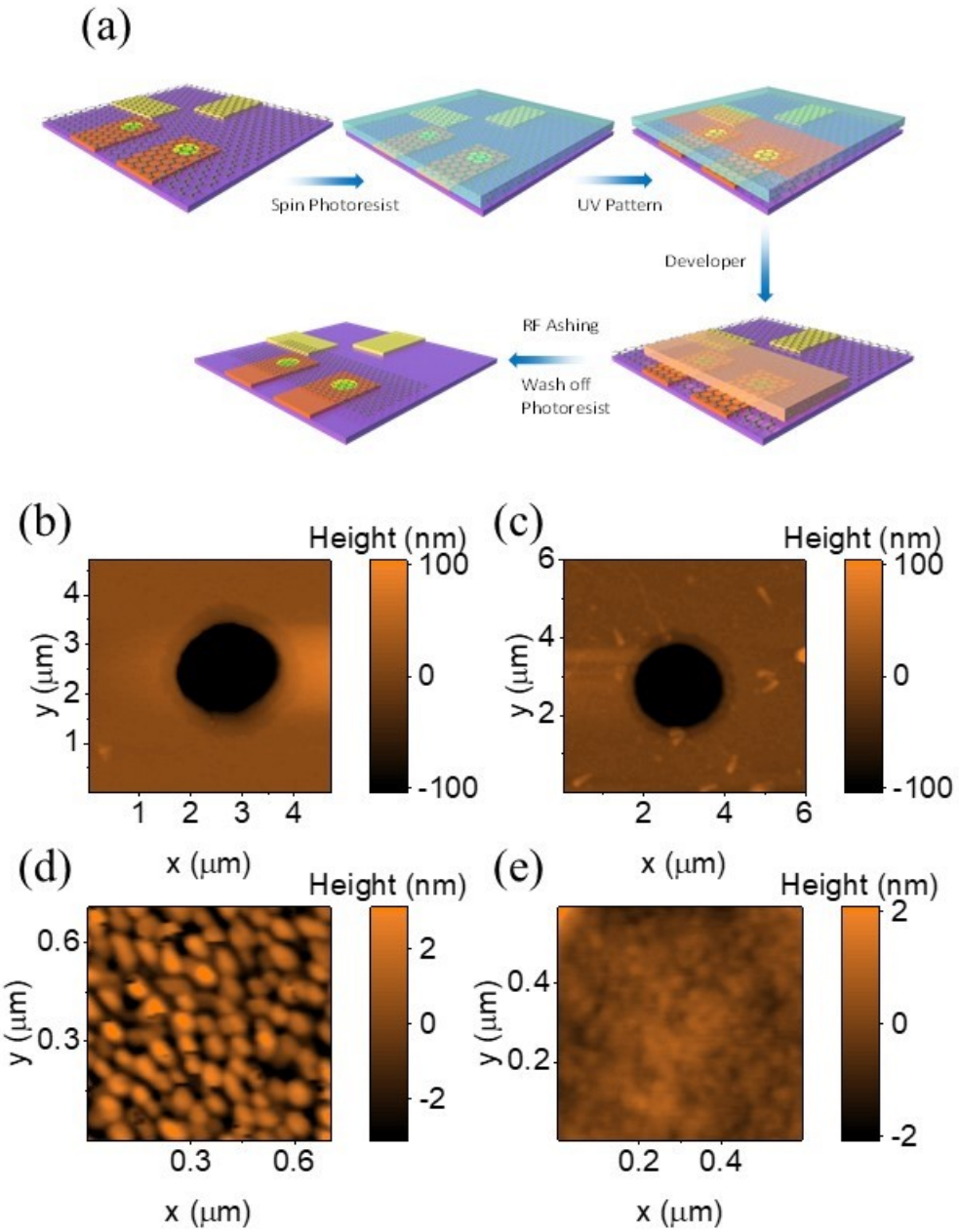

Figure S3. (a) Flow chart of junction formation. (b, d) AFM image for micro-well and gold electrode before graphene transfer. (c, e) AFM image for micro-well and gold electrode after graphene transfer.

1.3 XPS measurement

5 nm titanium and 20 nm gold were evaporated onto a Si/SiO_2 substrate. The prepared Au sample was spin coated with S1805 photoresist, exposed under UV light (without shadow mask) and developed by the developer. The process was the same as mentioned in the Device Fabrication section, and was used to ensure that the photolithography process on the gold surface (mentioned in the Device Fabrication section) did not impact the SAM growth.

The pre-treatment and SAM growth procedure for XPS samples was the same as in the 'device pre-treatment' and 'SAM growth' sections.

X-ray photoelectron spectroscopy (XPS) analysis was carried out using a customized NAP-XPS spectrometer from SPECS Surface Nano Analysis GmbH (Berlin, Germany) that allows the possibility of doing measurements at pressures lower then 10^{-5} mBar. The instrument was operated in the fixed analyser transmission mode, a monochromatic Al-Kα source (1486.74 eV) and 90 W was used. Survey and narrow scans were acquired using pass energy of 20 eV. For all samples, 3 survey scans were recorded using 1 eV steps and dwell time of 0.1 s. For narrow scans of C, Au, O, the number of scans was 2, using step size of 0.1 eV and dwell time of 0.5 s. For narrow scans of N and S the step size used was 0.05 eV, 0.5 s dwell time and 10 and 20 scans were recorded, respectively. The number of scans of C, Au, N, S for reference samples was 2 using the corresponding step sizes and dwell times as for the rest of the samples.

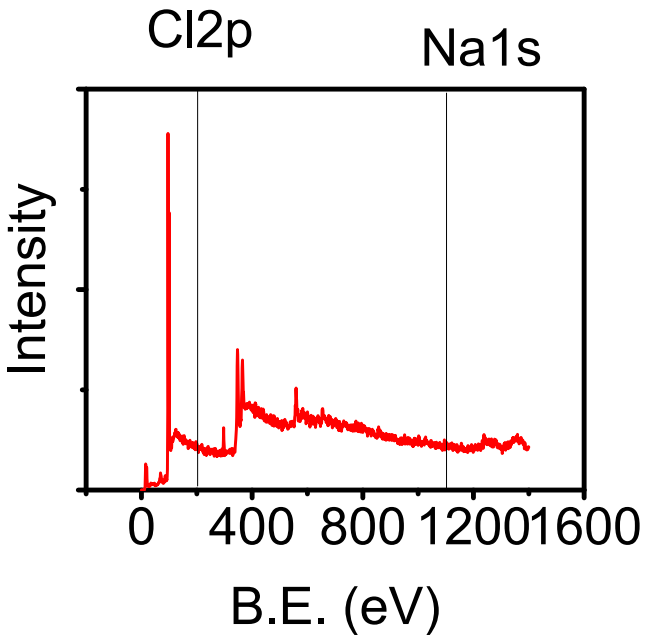

Figure S4. XPS survey scan on SAM 2, Cl2p and Na1s signal was not observed, means there is almost no ion remain due to deprotection procedure.

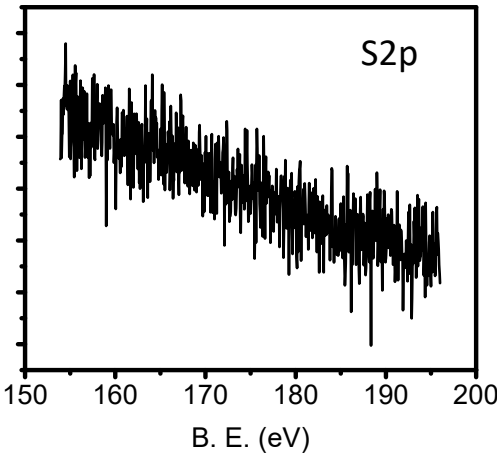

Figure S5. XPS result on gold immersed in DMF without molecules with same SAM grow method.

1.4 Electrical Measurement

The device after fabrication was wire-bonded to a leadless chip carrier, keeping the temperature at 35^{o}C. The bias voltage between source and drain (V_{SD}) was generated by a Keithley 2400 SMU.

The differential conductance (d*I*/d*V*) was obtained using a lock-in amplifier (SR830). A homemade DC/AC mixer was used to mix the DC voltage generated from the Keithley 2400 SMU (floating) and the AC voltage generated from the SR830's internal oscillator (grounded, 10 mV amplitude, 127 Hz frequency). The current was converted to a voltage signal using a Femto DLPCA 200 current pre-amplifier and measured by the SR830 lockin amplifier.

For each type of molecule, at least 2 independent batches of samples were prepared (using the same recipe) to assess reproducibility and detect unwanted one-off effects (contamination, low-quality graphene, bad SAM etc.). On occasions when data showed signs of bad SAM or graphene quality (many shorts or low Au/graphene/Au conductance), or the measured conductance had large disagreement with each other, more batches were prepared and measured.

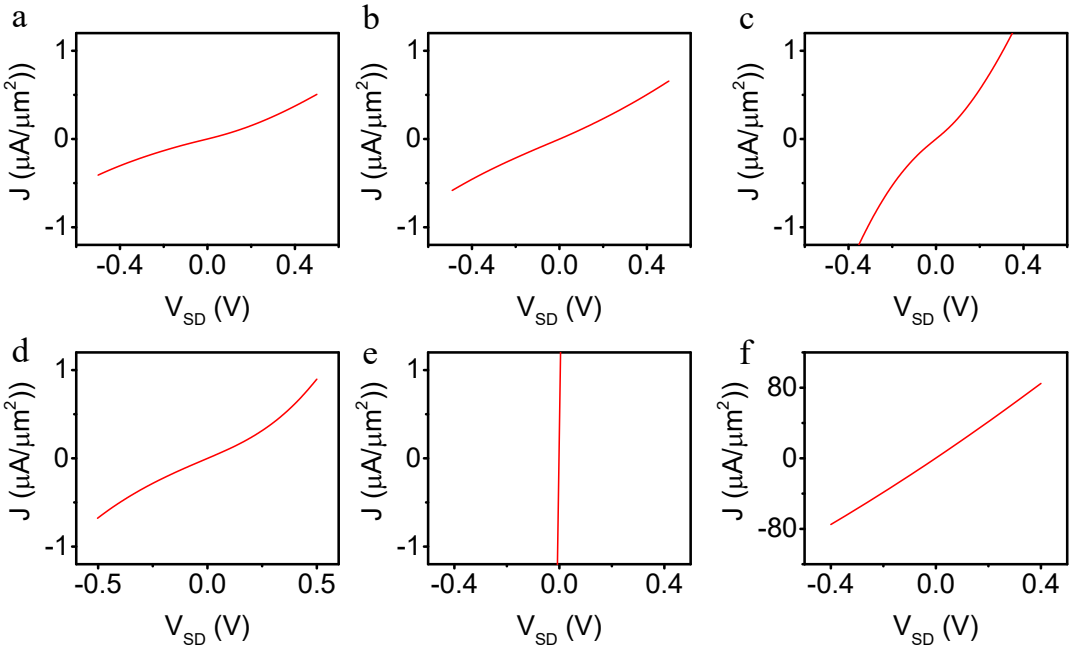

Figure S6. (a-d) Averaged IV curves for SAM 1-4, (e) IV curve for graphene without SAM. To clarify the comparison, y axis range was fixed. (f) IV curve for graphene without SAM in full y axis.

1.5 Fermi-level shift via Ionic liquid gating

The procedure of ionic liquid gating on device was reported in our previous paper [2], with leakage current, stability, and reproducibility verified. The measurement procedure was as following:

A small droplet of ionic liquid diethylmethylammonium bis(trifluoromethylsulfonyl)imide (DEME-TFSI, Sigma Aldrich, >98.5%, ~50 µL) was dropped onto the device. The device was checked in an optical microscope to ensure all the micro-wells and gate electrodes were covered by the ionic liquid. The leakage current between the gate and common contacts was checked before and after adding the ionic liquid drop. (Figure S7)

A second Keithley 2400 SMU was used to apply a series of gate voltages in the range where there was almost no leakage current. At each gate voltage, the junction was stabilized for 240 seconds, and then the SD voltage was applied and electrical transport was measured as described in the Electrical Measurement section (scan rate 300 mV/s). To establish that the molecules do not desorb from the electrodes, three IV curves were measured at each gate voltage for several cycles and the current remained constant; if desorption was occurring a rapid increase in current would be expected because of the short circuit between gold and graphene electrodes.. *I-V* characteristics of the junction at zero gate voltage were measured before and after applying the series of gate voltages, and also compared with the *I-V* curve before addition of the ionic liquid, to ensure that the ionic liquid and gate voltage did not destroy the junction. (Figure S8)

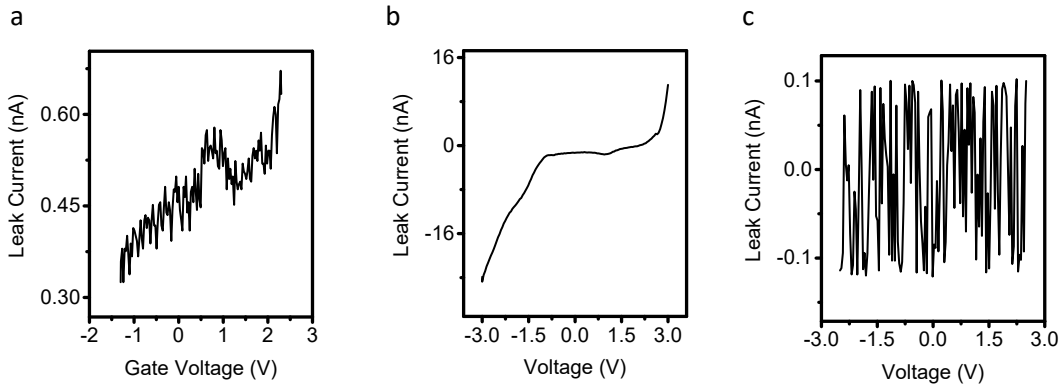

Figure S7. A typical example of gate-drain leakage current of an ionic liquid droplet for gate voltages from –1.3 to +2.3 V (a) and –3 to +3V (b), and the leakage current without ionic liquid droplet in the voltage range –2.5 to +2.5 V (c).

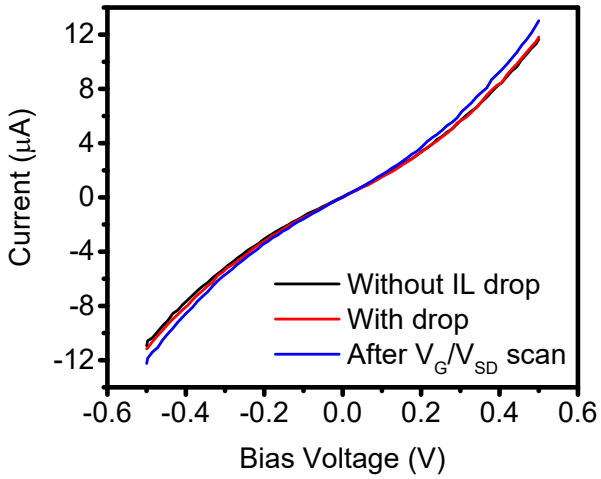

Figure S8. A typical example of an *I-V* curve of a molecular junction with SAM **1** at zero gate voltage, before (black) and after (red) adding the ionic liquid, and after the series scanning of conductance map *vs* V_{SD} and V_{gate}.

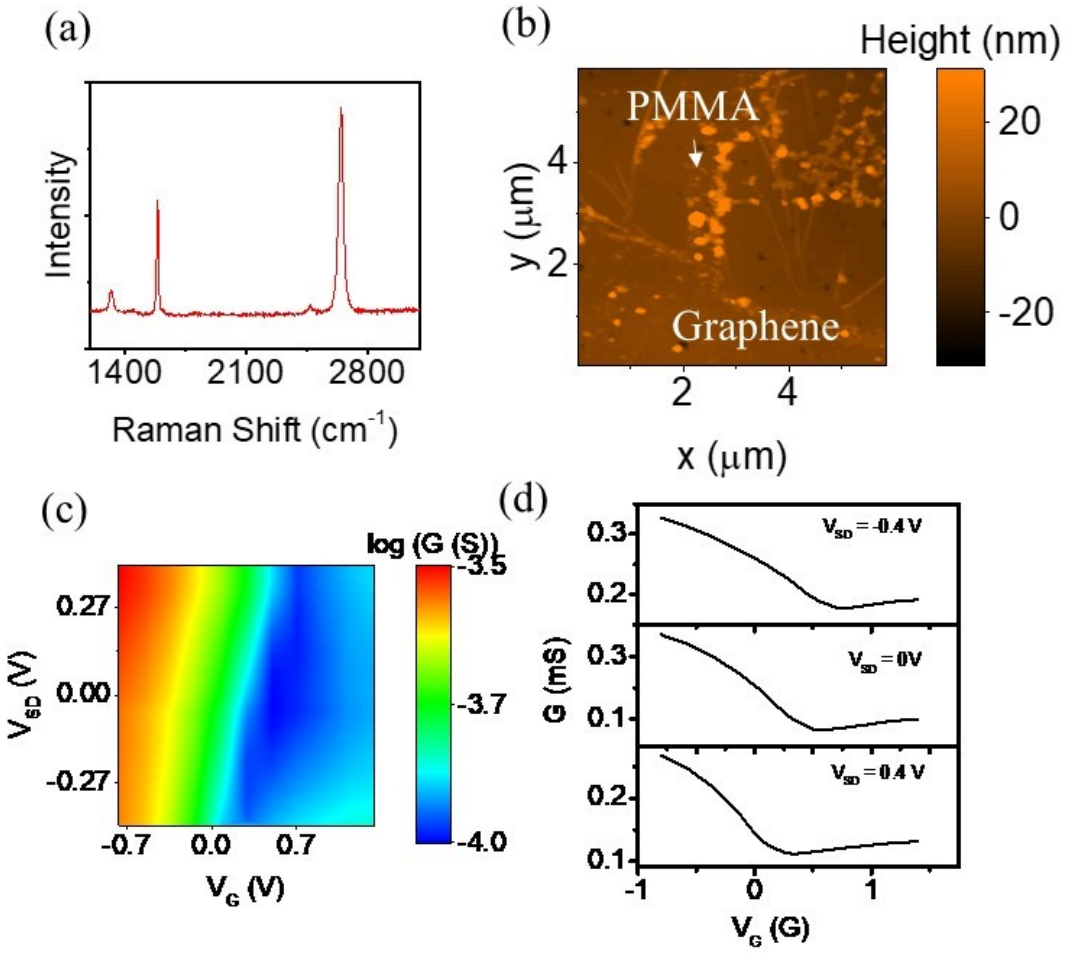

Figure S9. Characterization of chemical vapor deposition (CVD) graphene used in this study. (a) Raman spectrum of graphene transferred onto the device (operated on SiO2 region). (b) AFM topography image of graphene. (c) Shift of in-plane conductance of graphene by changing source-drain and gate voltages. (d) Change in gate voltage at three typical source-drain voltage points.

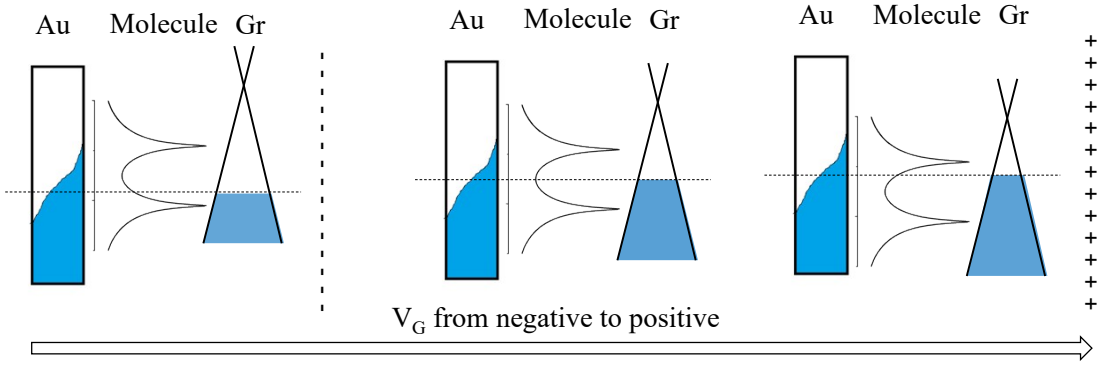

Figure S10. Illustration of energy diagram for SAM 1 under gate voltage control.

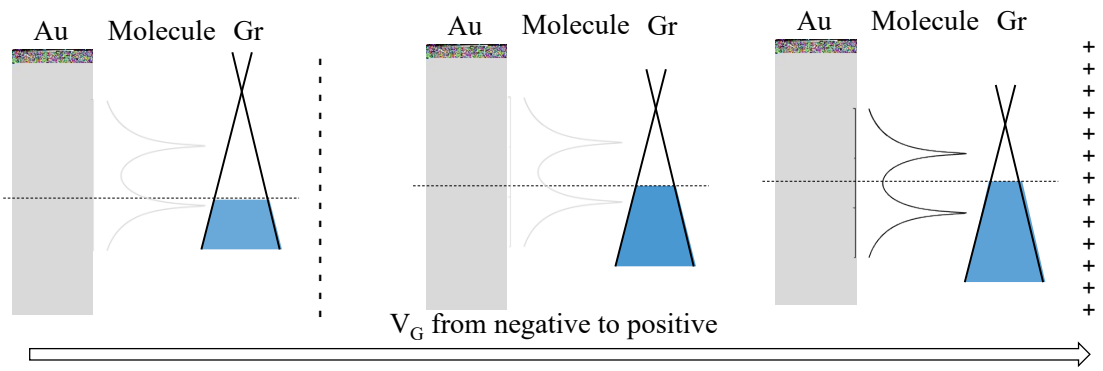

Figure S11. Illustration of energy diagram for SAM 2 (also same for 3 and 4) under gate voltage control.

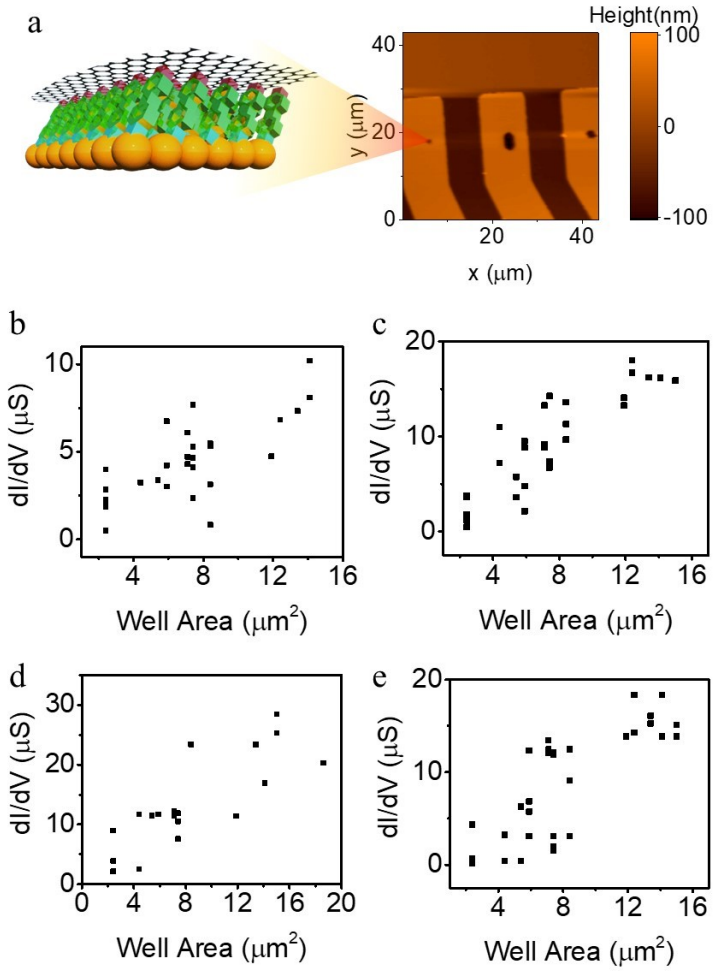

Figure S12: (a) An AFM image of micro-chip used in this work, molecules were grown in the micro-wells, and the micro-well were designed with different area, (b-d) plot of measured dI/dV vs. well area for SAM **1-4**, respectively.

Table S1. Total junction, surviving rate, short circuit rate and open circuit rate for SAM 1-4.

Device Number	SAM	Total Junction	Survive	Short	Open
1-1	SAM 1	16	11(69%)	5(31%)	0(0%)
1-2	SAM 1	16	11(69%)	5(31%)	0(0%)
1-3	SAM1	16	14(87.5%)	2(12.5%)	0(0%)
1-4	SAM1	16	12(75%)	3(19%)	1(6%)
2-1	SAM2	16	13(81%)	3(19%)	0(0%)
2-2	SAM2	16	13(81%)	3(19%)	0(0%)
3-1	SAM3	16	7(44%)	9(56%)	0(0%)
3-2	SAM3	16	11(69%)	5(31%)	0(0%)
4-1	SAM4	16	16(100%)	0(0%)	0(0%)
4-2	SAM4	16	12(75%)	4(25%)	0(0%)

Table S2. Absolute conductance (in $S/\mu m^2$) for SAM 1-4.

SAM	Exp. G ($S/\mu m^2$)	Std ($S/\mu m^2$)
1	0.56	0.27
2	1.05	0.35
3	2.27	0.42
4	1.1	0.39

Table 3. S:C atomic ratio from XPS atomic ratio analysis and expected value.

	S:C (XPS)	S:C (Expected)
SAM1	1:14.2	1:13.5
SAM2	1:13.2	1:13
SAM3	1:13.6	1:13
SAM4	1:13.2	1:13

2. Theoretical details

2.1 Optimized DFT Structures of Isolated Molecules

Using the density functional code SIESTA,[5, 6] the optimum geometries of the isolated molecules **1**-**2** were obtained by relaxing the molecules until all forces on the atoms were less than 0.01 eV / Å as shown in Fig. S16. A double-zeta plus polarization orbital basis set, norm-conserving pseudopotentials, with an energy cut-off of 250 Rydbergs, defined on the real-space grid was used and the local-density approximation (LDA) was chosen to be the exchange-correlation functional. We also computed results using GGA and found that the resulting transmission functions were comparable with those obtained using LDA.[7, 8]

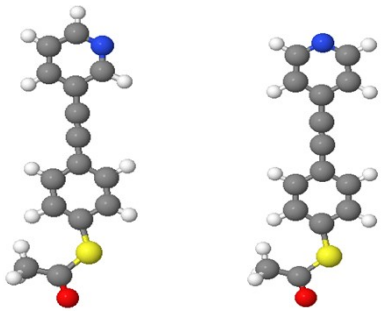

1 **2**

Figure S13. Fully relaxed isolated molecules **1** and **2**. Key: C = grey, H = white, O = red, S = yellow, N=blue.

2.2 Frontier orbitals of the molecules

The plots below (Figs. S11–S12) show isosurfaces of the HOMO, LUMO, HOMO–1 and LUMO+1 of isolated molecules **1-2** along with their energies.

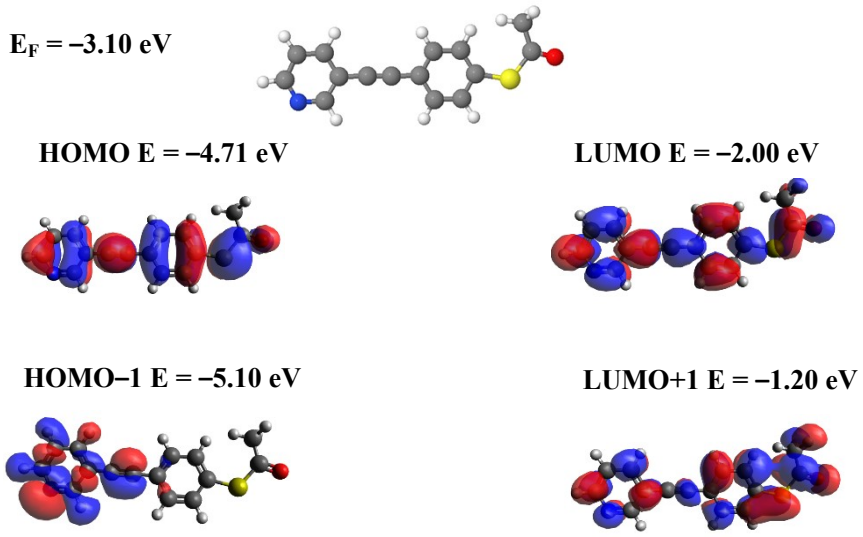

Figure S14. Wave function for molecule **1**. Top panel: Fully optimized geometry of molecule **1**. Lower panel: HOMO, LUMO, HOMO–1 and LUMO+1 along with their energies.

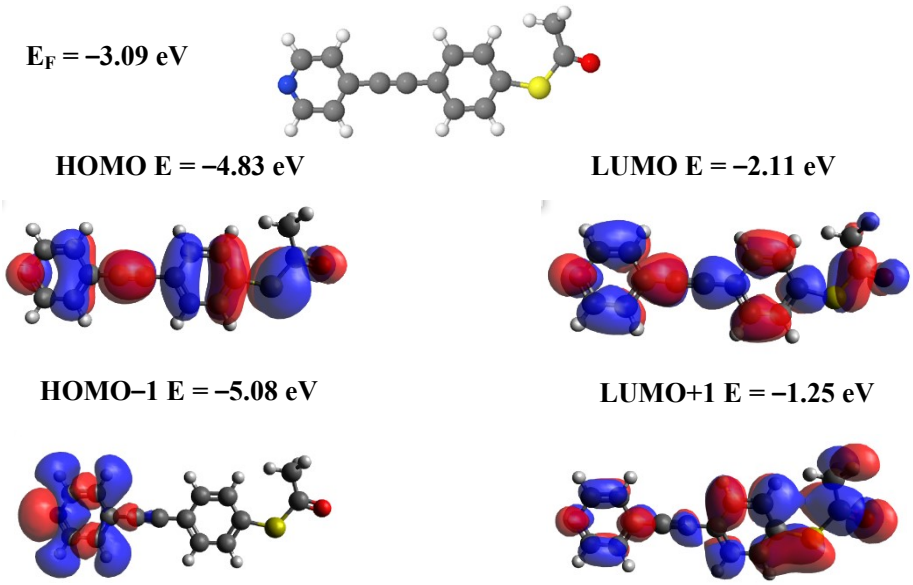

Figure S15. Wave function for molecule **2**. Top panel: Fully optimized geometry of molecule **2**. Lower panel: HOMO, LUMO, HOMO–1 and LUMO+1 along with their energies.

2.3 Binding energies of molecules on graphene and gold

To calculate the optimum binding distance between the anchor groups and electrodes, we used DFT and the counterpoise method, which removes basis-set superposition errors (BSSE). The binding distance *z* is defined as the distance between the top or bottom surface and the anchor group (see the black double-arrow on the right panel of Figs. S13-S16).

We define one of the compounds **1-2** as entity A and the single-layer graphene (SLG) or gold electrode as entity B. The ground-state energy of the total system is calculated using SIESTA and is denoted E_{AB}^{AB}. The energy of each entity is then calculated in a fixed basis, which is achieved using ghost atoms in SIESTA. Hence, the energy of the individual molecule **1-2** in the case of the fixed basis is defined as E_{A}^{AB} and for the graphene/gold as E_{B}^{AB}. The energy difference $\Delta(z)$ between the isolated entities and their total energy when placed a distance z apart is then calculated using the following equation:

$$Energy\ difference = \Delta(z) = E_{AB}^{AB} - E_{A}^{AB} - E_{B}^{AB} \ . \qquad \text{(S1)}$$

The energy differences are shown as a function of separation z in Figs. S13-S16 for molecules **1-2** with the equilibrium distance z, corresponding to the minimum energy difference to the electrode, tabulated in Table S5. Here, the energy difference has been calculated for two different contact electrodes. The top contact is graphene-molecule (Gr-M), whereas the bottom contact is gold-molecule (Au-M).

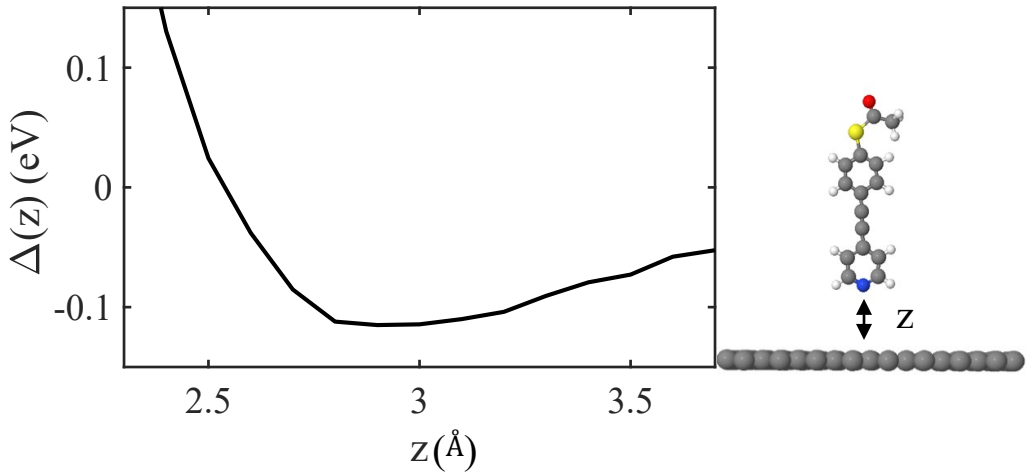

Figure S16. Pyridine anchor (molecule **2**) on a graphene surface (Right panel). Energy difference of pyridine anchor to graphene as a function of molecule-contact distance. The equilibrium distance is approximately 2.7 Å (Left panel).

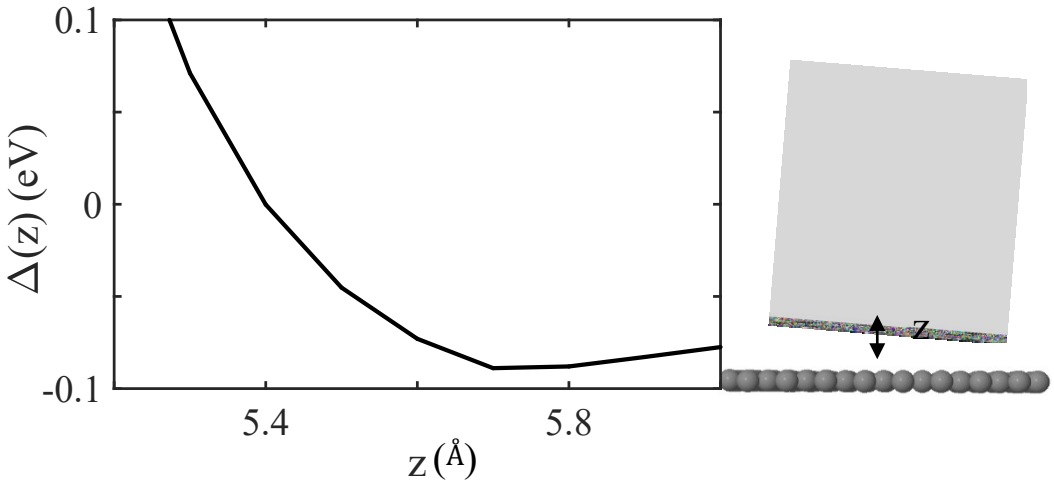

Figure S17. Thioacetate anchor (molecule **2**) on a graphene surface (Right panel). Energy difference of thioacetate anchor to graphene as a function of molecule-contact distance. The equilibrium distance is approximately 5.7 Å (Left panel).

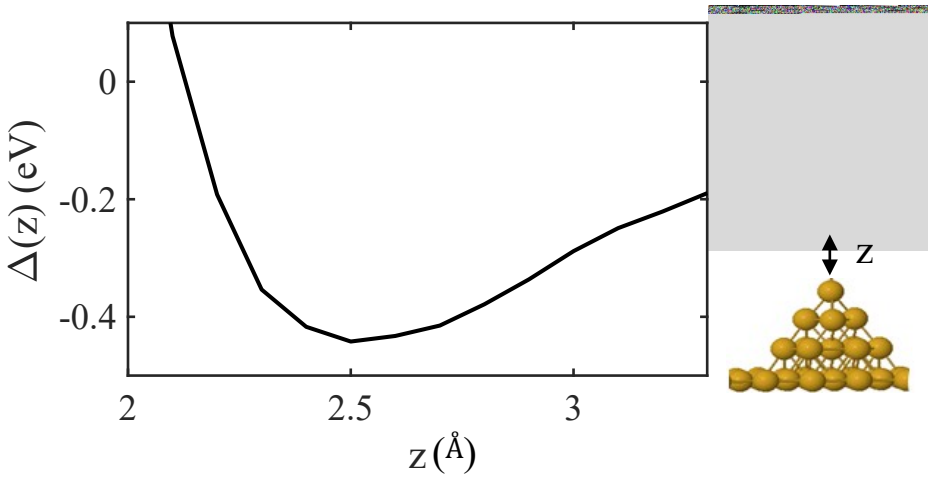

Figure S18. Pyridine anchor (molecule **2**) on a gold surface (Right panel). Energy difference of pyridine anchor to gold as a function of molecule-contact distance. The equilibrium distance is approximately 2.5 Å (Left panel).

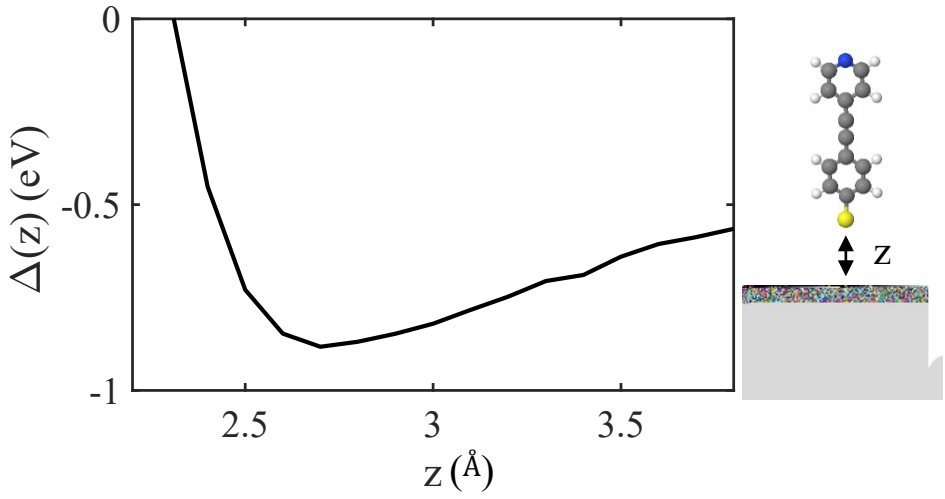

Figure S19. Thiolate anchor (molecule **2**) on a gold surface (Right panel). The acetyl protecting group has been released. Energy difference of thiolate anchor to gold as a function of molecule-contact distance. The equilibrium distance is approximately 0.27 nm (Left panel).

Table S4: Summary of the energy-difference calculations (Figs. S13-S16) for graphene-molecule (Gr-M) and gold-molecule (Au-M) contacts. *z* is the equilibrium distance and $\Delta(z)$ is the corresponding minimum energy difference.

Compound	$\Delta(z)$ **(eV)**	***z*** **(Å)**
Gr-Pyridine	0.14	2.7
Gr-Thioacetate	0.09	5.7
Au-Pyridine	0.42	2.5
Au-Thiol	0.69	4.2

2.4 Optimized DFT structures of compounds within their junctions

Using the optimized structures and geometries for the compounds obtained as described above, we again employed the SIESTA code to calculate self-consistent optimized geometries, ground-state Hamiltonians and overlap matrix elements for each graphene-molecule-gold

junction. The optimized structures were then used to compute the transmission curve for each compound. The DFT-optimized geometries are shown in Fig. S17. Note that there is a tilt-angle range for each compound, which is presented in section 2.5.

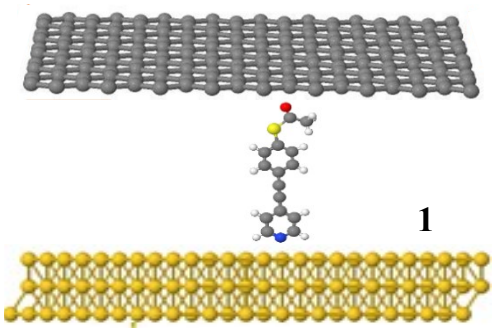
1

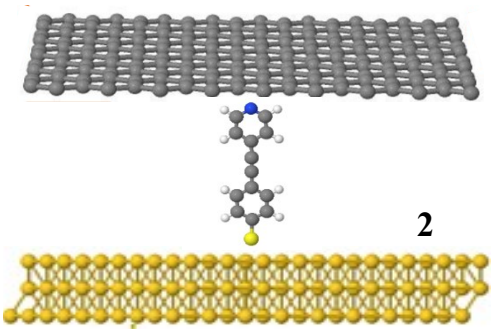
2

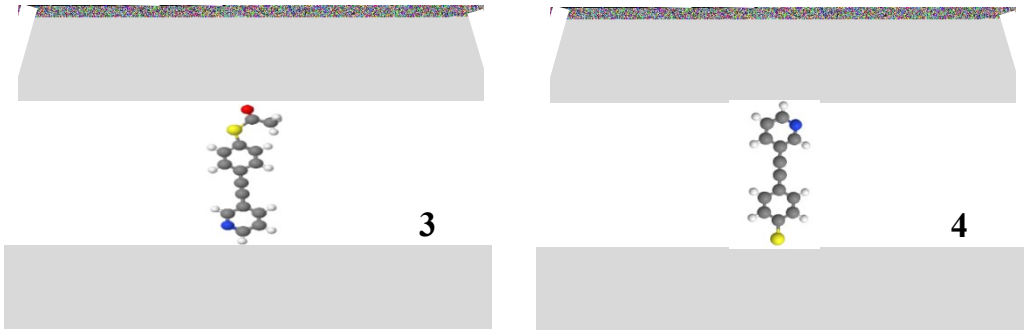

Figure S20. Schematic illustration of junctions containing a single molecule **1-2**. (The nomenclature a and b for molecules **2** and **3** refers to the binding motif, as in manuscript Figure 2). The top contact is single-layer graphene (SLG) and the bottom contact is gold.

2.5 Tilt angle

In this section, we determine the tilt angle θ of each compound and binding motif between SLG and a gold substrate, which corresponds to the experimentally measured most-probable break-off distance. Table S6 shows a range of tilt angles calculated from the film thickness for each molecule. Break-off distance values suggest that compounds **1**, **2**, **3**, and **4** tilt at an angle θ ranging from 37° to 47° and compound **2b** tilts at 63° to 73°, as shown in Fig. S18.

Table S5: Experimental break-off distances and equivalent tilt angles (θ)

Compound and binding motif	**Experimental film thickness (nm)**	**Equivalent experimental tilt angle (θ)**	**Equivalent theoretical tilt angle (θ)**
1	1.05	37°-47°	37°-47°
2		63°-73°	63°-73°
3	0.7	37°-47°	37°-47°
3		12°-20°	12°-20°

4	1.1	37°-49°	37°-49°

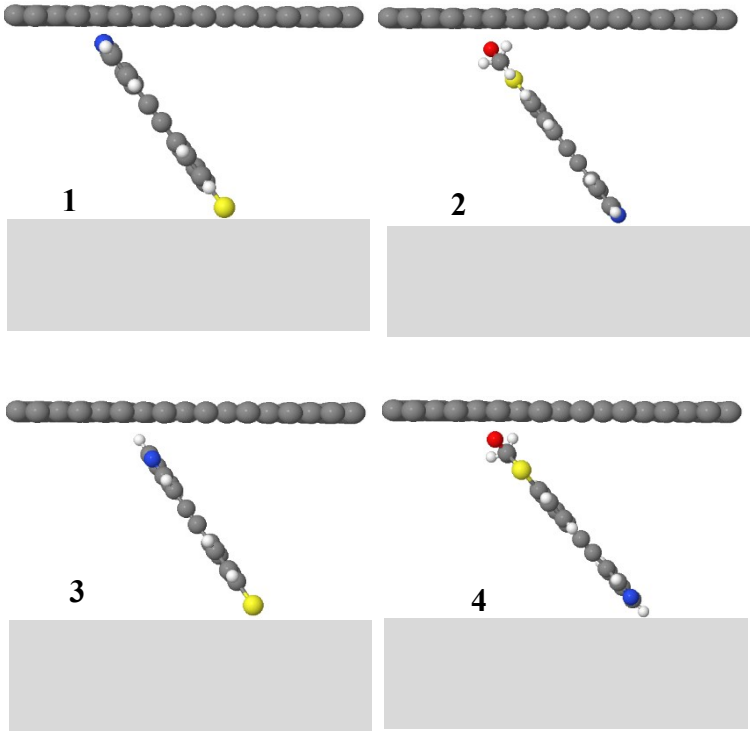

Figure S21. Tilt angle of structures **1**-**2**.

2.6 DFT-based transport calculations

In the following transport calculations, the ground-state Hamiltonian and optimized geometry of each compound was obtained using the density-functional theory (DFT) code.[5] The local-density approximation (LDA) exchange-correlation functional was used along with double-zeta-polarized (DZP) basis sets and the norm-conserving pseudo-potentials. The real-space grid was defined by a plane-wave cut-off of 250 Ry. Geometry optimization was carried out to a force tolerance of 0.01 eV/Å. This process was repeated for a unit cell with the molecule between graphene and gold electrodes where the optimized distances between SLG/Au and the anchor groups are shown in Table S5. From the ground-state Hamiltonian, the transmission coefficient, and hence the room-temperature electrical conductance G, were obtained as described in the sections below. We modelled the properties of a single molecule in the junction, as previous works[9] have shown that the calculated conductance per molecule of a SAM differs only slightly from that of single molecules.

2.7 Transport calculations in a three-terminal junction

To calculate the electrical transport through a SAM (**1-2**), we modelled the three-terminal junction shown in the top panel of Fig. S31. The in-plane periodicity of the graphene and the molecular

layer is achieved by repeating the unit cell using a Bravais lattice with 50k points in the *y*-direction (see upper black arrow). The gold electrode is modelled as a nanowire attached to each molecule. A mean-field Hamiltonian and an overlap matrix were extracted from the converged DFT calculation and combined with our quantum-transport calculation code, Gollum, to calculate the transmission coefficient $T(E)$ of electrons of energy E passing from the graphene to the gold electrode.

In the three-terminal junction, there are two transmission functions 1-3 and 2-3 describing transport between the gold and graphene electrodes.

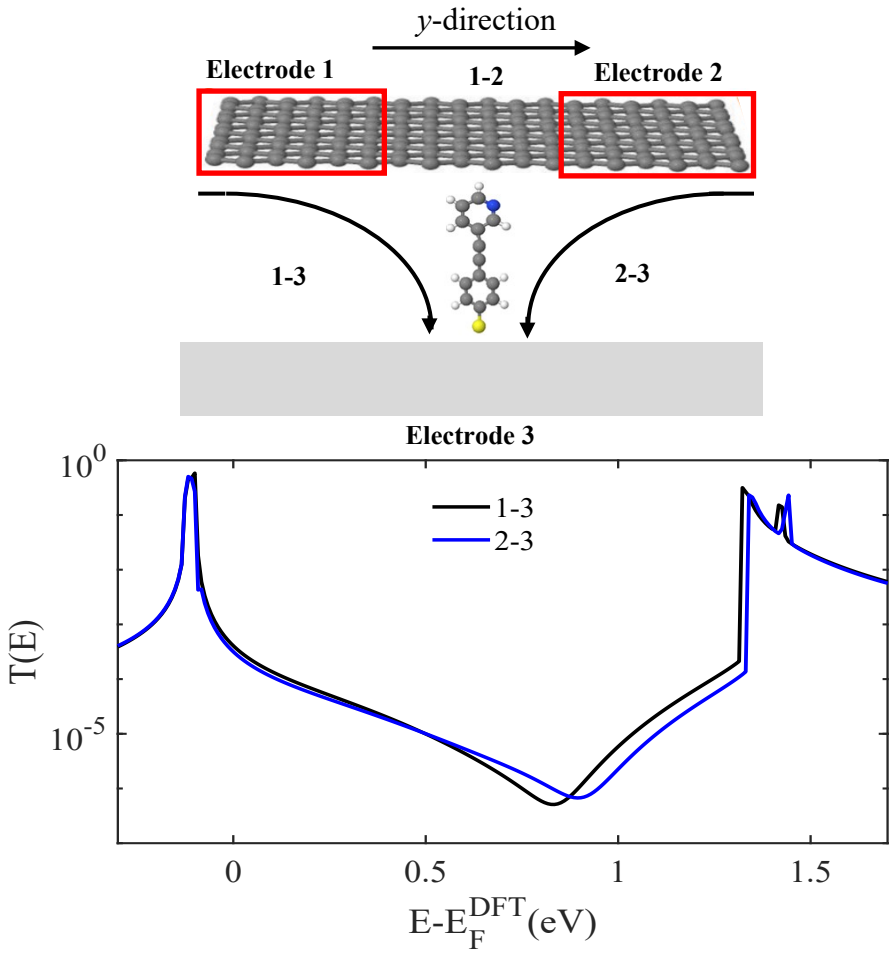

Figure S22. Top panel: schematic illustration of a three-terminal Au/**1**/SLG junction with periodic boundary conditions along the *y*-axis. The top contact is SLG and is divided into two electrodes (electrode 1 and electrode 2), whereas the bottom contact is Au (electrode 3). Bottom panel: an example of zero-bias transmission coefficient $T(E)$ curves: 1-3 and 2-3 have equal path lengths, and therefore have identical curves (black and blue lines).

Since the two paths 1-3 and 2-3 yield almost identical transmission coefficients $T(E)$, the average of them is shown in Figures S20-S21. Fig. S20 shows the average transmission

coefficient $T(E)$ for SAM **1**, whose tilt angle is 40°.

As shown in the upper panel of Fig. S21, for **1**, there are two possible binding configurations (motifs) in the junction. For **1a** the (deprotected) thiolate binds to Au and pyridine binds to SLG, and for **1b** the molecule is flipped vertically in the junction, with the pyridine binding to the gold and the (protected) thioacetate to the SLG. As expected **1b** yields lower conductance (bottom panel), because the separation between the Au and SLG electrodes is larger than in **1a**.

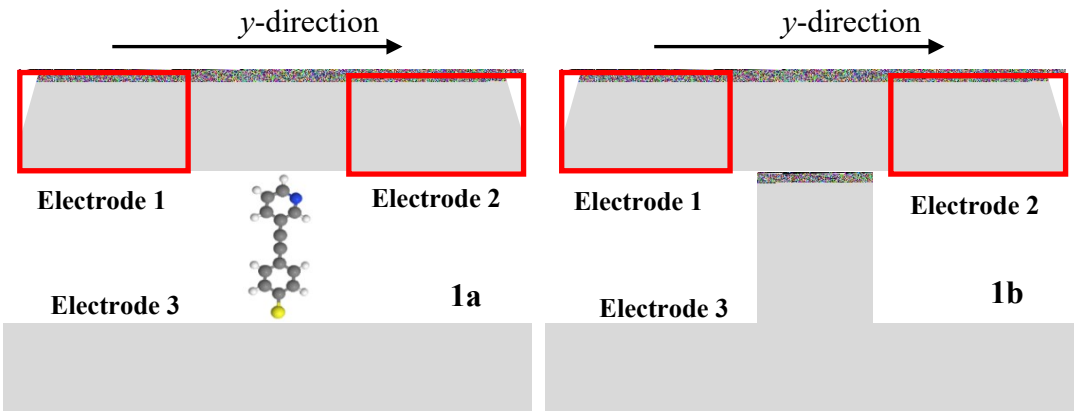

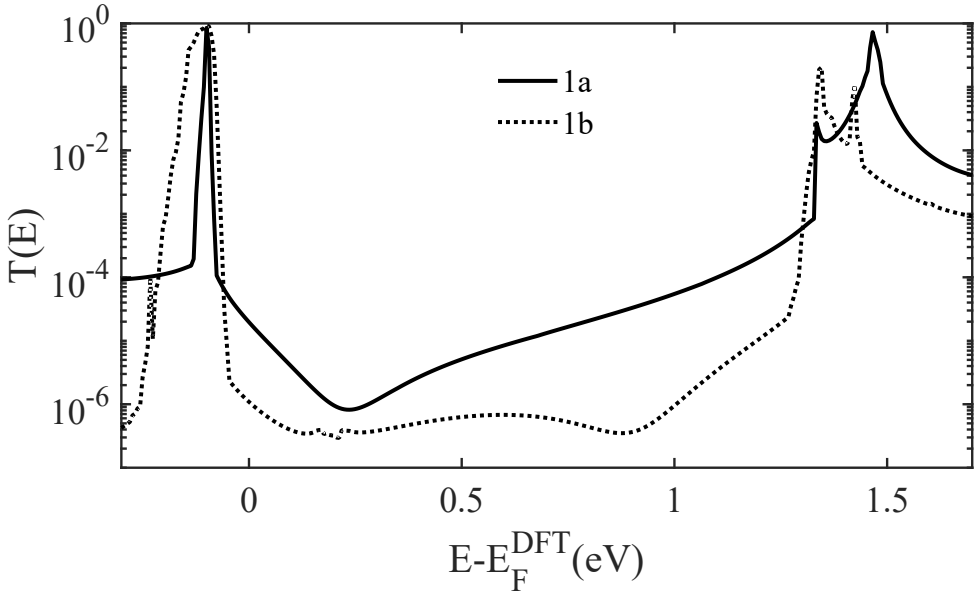

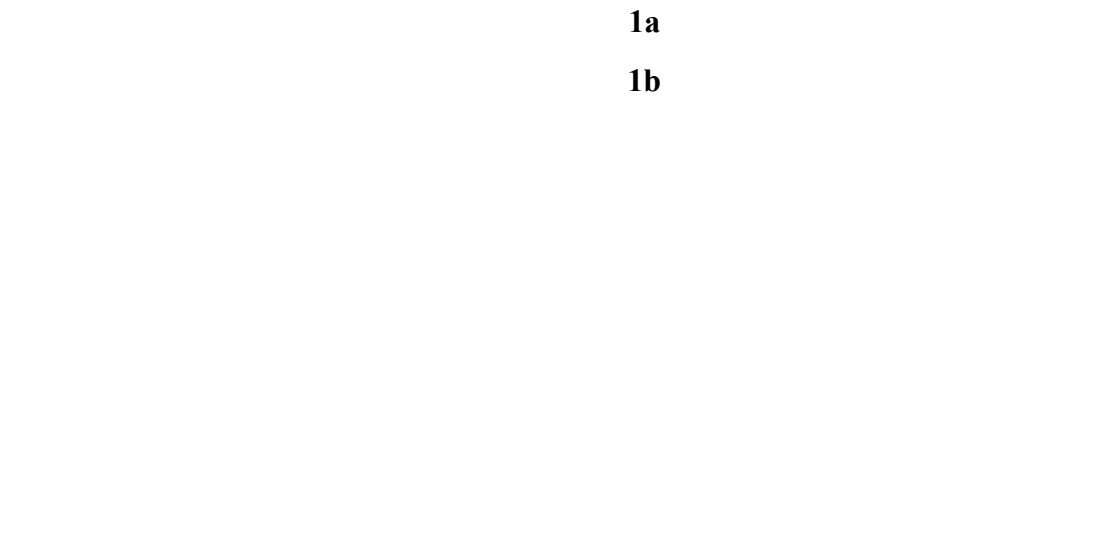

Figure S23. Top panel: schematic illustration of a three-terminal Au/**1a** or **1b**/SLG junction with periodic boundary conditions along the *y*-axis, as in Fig. S19. Bottom panel: zero-bias transmission coefficient $T(E)$ averaged over the values for paths 1-3 and 2-3.

Similarly, **2** also has two possibilities in the junction. Configuration **2a** occurs when the thiolate binds to Au and pyridine binds to SLG, and **2b** when the molecule is flipped vertically in the junction, with the pyridine binding to Au and the thioacetate to the SLG as shown in the top panel of Fig. S21. **2b** yields a lower conductance (bottom panel), because the separation between the Au and SLG electrodes is larger than in **2a**.

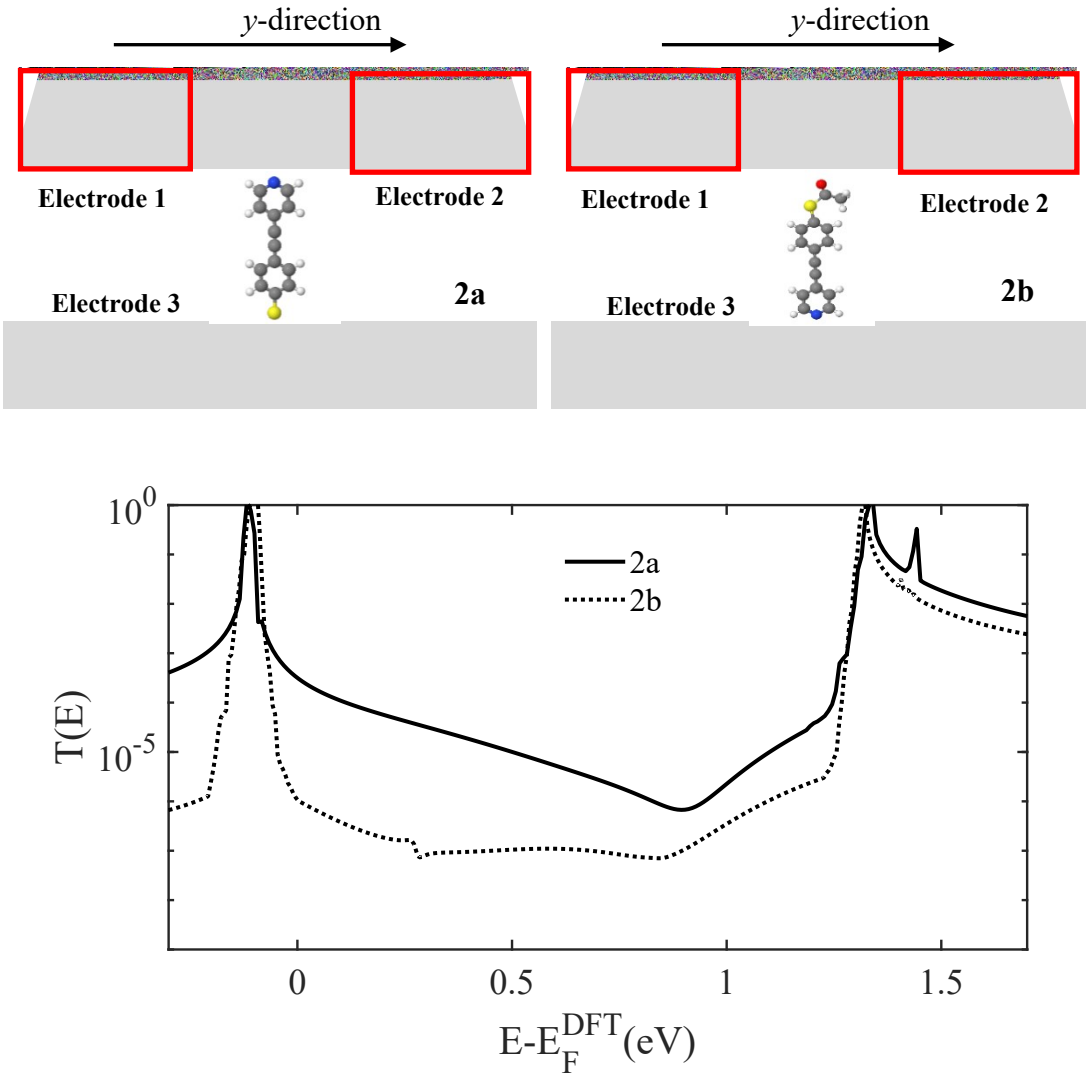

Figure S24. Top panel: schematic illustration of a three-terminal Au/**2a** or **2b**/SLG junction with periodic boundary conditions along the *y*-axis, as in Fig. S19. Bottom panel: zero-bias transmission coefficient $T(E)$ averaged over the values for paths 1-3 and 2-3.

References

1. L. J. O'Driscoll, X. T. Wang, M. Jay, A. S. Batsanov, H. Sadeghi, C. J. Lambert, B. J. Robinson and M. R. Bryce, Carbazole-Based Tetrapodal Anchor Groups for Gold Surfaces: Synthesis and Conductance Properties, *Angewandte Chemie-International Edition*, 2020, **59**, 882-889.
2. X. T. Wang, A. Ismael, S. L. Ning, H. Althobaiti, A. Al-Jobory, J. Girovsky, H. P. A. G. Astier, L. J.

O'Driscoll, M. R. Bryce, C. J. Lambert and C. J. B. Ford, Electrostatic Fermi level tuning in large-scale self-assembled monolayers of oligo(phenylene-ethynylene) derivatives, *Nanoscale Horiz*, 2022, **7**, 1201-1209.

3. C. Vericat, M. E. Vela, G. Benitez, P. Carro and R. C. Salvarezza, Self-assembled monolayers of thiols and dithiols on gold: new challenges for a well-known system, *Chem Soc Rev*, 2010, **39**, 1805-1834.
4. A. Ibrahim, G. Nadhreen, S. Akhtar, F. M. Kafiah and T. Laoui, Study of the impact of chemical etching on Cu surface morphology, graphene growth and transfer on SiO2/Si substrate, *Carbon*, 2017, **123**, 402-414.
5. J. M. Soler, E. Artacho, J. D. Gale, A. García, J. Junquera, P. Ordejón and D. Sánchez-Portal, The SIESTA method for ab initio order-N materials simulation, *Journal of Physics: Condensed Matter*, 2002, **14**, 2745.
6. E. Artacho, E. Anglada, O. Diéguez, J. D. Gale, A. García, J. Junquera, R. M. Martin, P. Ordejón, J. M. Pruneda and D. J. J. o. P. C. M. Sánchez-Portal, The SIESTA method; developments and applicability, 2008, **20**, 064208.
7. A. K. Ismael and C. J. Lambert, Single-molecule conductance oscillations in alkane rings, *Journal of Materials Chemistry C*, 2019, **7**, 6578-6581.
8. M. Gantenbein, L. Wang, A. A. Al-Jobory, A. K. Ismael, C. J. Lambert, W. Hong and M. R. Bryce, Quantum interference and heteroaromaticity of para-and meta-linked bridged biphenyl units in single molecular conductance measurements, *Scientific reports*, 2017, **7**, 1-9.
9. L. Herrer, A. Ismael, S. Martin, D. C. Milan, J. L. Serrano, R. J. Nichols, C. Lambert and P. Cea, Single molecule vs. large area design of molecular electronic devices incorporating an efficient 2-aminepyridine double anchoring group, *Nanoscale*, 2019, **11**, 15871-15880.